Title: MR Imaging of the Aorta

Ichiro Sakamoto, MD[a], Eijun Sueyoshi, MD[b], and Masataka Uetani, MD[c]

a) Assistant Professor of Department of Radiology and Radiation Biology, Nagasaki University Graduate School of Biomedical Sciences

b) Research Assistant of Department of Radiology and Radiation Biology, Nagasaki University Graduate School of Biomedical Sciences

c) Professor and Chairman of Department of Radiology and Radiation Biology, Nagasaki University Graduate School of Biomedical Sciences

Keywords: MR, Angiography, Aorta, Aneurysm, Dissection

[a]Corresponding author for proof and reprints:

Ichiro Sakamoto, MD

Department of Radiology and Radiation Biology, Nagasaki University Graduate School of Biomedical Sciences, 1-7-1 Sakamoto, Nagasaki 852-8501, Japan.

TEL: 81-95-849-7355, FAX: 81-95-849-7357, E-mail: ichiro-s@net.nagasaki-u.ac.jp

[b, c]Coauthors addresses:

Eijun Sueyoshi, MD[b]

Department of Radiology and Radiation Biology, Nagasaki University Graduate School of Biomedical Sciences, 1-7-1 Sakamoto, Nagasaki 852-8501, Japan.

TEL: 81-95-849-7355, FAX: 81-95-849-7357

Masataka Uetani, MD[c]

Department of Radiology and Radiation Biology, Nagasaki University Graduate School of Biomedical Sciences, 1-7-1 Sakamoto, Nagasaki 852-8501, Japan.

TEL: 81-95-849-7355, FAX: 81-95-849-7357

Introduction

Acquired disease of the aorta is widespread and required invasive angiography to depict structural abnormalities in the past. Recent advances in noninvasive imaging methods, such as CT and MR imaging, have replaced most of invasive angiographic procedures, thus resulting in decreasing the cost and morbidity of diagnosis [1-8]. With its ability to

the intrinsic contrast between blood flow and vessel wall, and acquire images in multiple planes, MRI provides a high degree of reliability in the diagnosis of aortic diseases. Since MRI can repeatedly be performed due to its totally noninvasive nature, the progression of the aortic disease can be evaluated over time. In this article, present MR imaging methods for evaluation of the aorta are reviewed and illustrated. Common diseases of the aorta will also be discussed focusing on their unique morphologic and functional features, and characteristic MR findings. Knowledge of pathologic conditions of common aortic diseases and proper MR techniques will enable accurate and time-efficient aortic MR evaluation.

Comparison with CT

Compared with MR angiography, CT angiography has the advantages of great general availability and ease of performance, especially in urgent cases. Nevertheless, MR imaging has several distinct advantages over CT. First, MR imaging dose not require the use of ionizing radiation. Due to the lack of radiation, MR imaging can repeatedly be performed for the follow-up of the patient without radiation exposure concerns. Second, unlike CT angiography, MR angiography dose not require the use of nephrotoxic iodinated contrast material. Nephrotoxicity is a particularly relevant issue, because the patients with acquired aortic disease frequently suffer from renal insufficiency. In particular, MR angiography has benefits for patients undergoing endovascular treatment. Preprocedural planning using MR angiography excludes the concerns related to iodine load and impaired renal function, thus enabling same day or close performance of endovascular treatment [7]. Finally, cine MR imaging can be performed for dynamic evaluation of blood flow without using contrast material. Particularly, cine phase-contrast can be used to

determine flow velocity and direction. These cine MR techniques can be used to evaluate valvular and cardiac function.

Basic technical considerations

Several different MRI imaging techniques are used to depict the arteries. These include black-blood imaging (conventional spin echo, fast spin echo), bright-blood imaging (time-of-flight imaging, phase-contrast imaging), and contrast-enhanced MR angiography. Recent advances in fast imaging, such as steady state free precession (SSFP) and subsecond contrast-enhanced MR angiography, enable quick examinations for initial screening evaluations of the aorta within several minutes. These improvements in MR technology and the aforementioned advantages of MR imaging over CT evaluation have increased role of MR angiography, even in the evaluation of some acute conditions.

Black-blood vascular imaging

The aorta can be well illustrated using black blood methods, namely, ECG-gated spin echo or fast spin echo (FSE) that exploits inherent contrast between rapidly flowing blood and the aortic wall [7, 9-12]. Unlike in bright blood imaging, luminal signal void occurs owing to movement of spins and dephasing of turbulent flow. Spin echo imaging still constitutes the basis of any aortic study because this technique provides the best anatomic details of the aortic wall and pathologic conditions. Usually, a conventional study of the aorta is first acquired in the axial plane to display the orientation of the great arteries and optimally visualize mural lesions perpendicular to their long axes. A main consideration in spin echo imaging is that each section corresponds to a different cardiac phases. Diastolic slow flow and entry or exit slice phenomena may produce high signal in the aortic lumen, which is difficult to differentiate from mural thrombus. Usually, T2-weighted imaging is of little utility in the study of the aorta since the low signal-to-noise ratio and the long acquisition time affect the image quality mainly due to motion artifact. Using spin echo imaging, not only aortic caliber but also the vessel wall and perivascular structures can be evaluated. Wall thickness can be readily demonstrated on T1-weighted imaging, and edema is seen as hyperintense

intramural signal on T2-weighted imaging. Mural hyperenhancement of the vessel wall on T1-weighted images after injection of contrast material is considered to indicate active inflammation. ECG-gated double inversion recovery (DIR) FSE is a more recent black blood method that allows breath hold acquisition [13]. By applying a nonselective inversion pulse followed by a section-selective inversion pulse, DIR FSE provides better suppression of the signal from flowing blood (Fig. 1). However, this technique is substantially less efficient in terms of scan time than FSE technique because it is a sequential-slice imaging sequence.

Bright blood vascular imaging

Several bright blood techniques can be done without the need for contrast agents [7, 14-17]. One of the oldest techniques is the time-of-flight (TOF) effect, which is based on the phenomenon of flow-related enhancement of spins entering into a partially saturated imaging section. These unsaturated spins give more signal than surrounding stationary spins. With the 2D technique, multiple thin, sequential sections are acquired by using a flow-compensated gradient echo sequence. The acquired sections are either viewed individually or reformatted with the MIP technique to obtain a 3D image. TOF imaging has the following several limitations [18,19]: (1) complex flow pattern producing loss of signal due to intravoxel dephasing may mimic disease; (2) vessels not perpendicular to the acquired section plane may show low signal intensity; (3) retrograde flow in collateral vessels may also be saturated, obscuring the true level of steno-occlusive lesions. Although arterial signal can be improved with cardiac gating, imaging times become long and arterial signal on TOF MR angiography often remains inhomogenous and unreliable for proper depiction of the aorta and its branches. Due to the long imaging times and aforementioned limitations, TOF imaging has been rapidly replaced with contrast-enhanced MR angiography.

The TOF effect can be useful when acquired in a 2D cine mode, for example, cine gradient echo (cine GRE) [7]. Cine GRE images are acquired with ECG gating, thus resulting in high temporal resolution throughout the cardiac cycle, and can be displayed in cine-format. Recently introduced SSFP (commercially known as true FISP, FIESTA, or balanced FFE) technique, with shorter TEs and TRs sequences, has become more widely available [16, 17]. On SSFP, intraluminal signal is

generally very high and homogenous even in cases of turbulent flow since this sequence depends mainly on a function of the T2/T1 ratio. Hence, in urgent situations, SSFP can be used to quickly demonstrate aortic abnormalities, such as an intimal flap and a false lumen in aortic dissection.

One critical advantage of flow-based bright blood techniques is the ability to perform a functional assessment of blood flow [7, 20, 21]. On cine GRE, turbulent flow produces rapid spin dephasing and results in flow jets extending distal to or downstream from the lesion, thus providing additional information in many pathologic conditions such as coarctation of the aorta, aortic valve insufficiency, and aortic dissection. Particularly in aortic dissection, the detection of entry and reentry sites is a special capability of this method that can be helpful in planning both surgical and endovascular treatment. With the use of newer fast GRE pulse sequences with an ultrashort TR and TE, a flow jet may not be present despite the presence of a significant flow disturbance (Reference?). The very short TE times may be insufficient for a sizable flow jet to form on this faster sequence. In cases of high suspicion, standard gradient echo pulse sequences can be performed during free breathing (Fig. 2) [7]. The longer TE will allow intravoxel dephasing to develop, and a flow jet should be seen if flow is turbulent.

Cine PC is another bright blood technique that can be used for dynamic evaluation of blood flow [7, 22, 23]. Cine PC depends on the phase shifts that flowing protons experience as they travel along the gradient field. The resulting data obtained with cine PC is processed into two sets of images: magnitude and phase-contrast. Phase- contrast images display the direction of flow as bright or dark pixels, with their relative signal intensity representing their velocity. Hence, phase contrast images can be used to assess flow direction, which may be important information for proper identification of a vascular structure or for quantifying blood flow.

Contrast-enhanced MR angiography

Contrast-enhanced MR angiography, which was first described for imaging of aortoiliac disease in 1993, is the most widely accepted method for comprehensive evaluation of the aortic disease [18, 24-26]. This technique can provide high spatial resolution images with a single breath

hold, and therefore is suitable for the depiction of aortic abnormalities such as aneurysm, dissection, penetrating atherosclerotic ulcer, and Takayasu arteritis.

Contrast-enhanced MR angiography uses T1-shortening effect of a gadolinium-based contrast agent. By using a gadolinium chelate contrast agent, the T1 of blood is shortened so that the blood appears bright irrespective of flow patterns or velocities. Since signal enhancement and overall image quality of contrast-enhanced MR angiography depend on the intraarterial contrast agent concentration, the correct timing of imaging after contrast material injection is crucial. Since image contrast depends mainly on central k-space data, collection of the central lines of k space during the plateau phase of arterial enhancement is essential for optimal contrast-enhanced MR angiography [27]. We use 10 - 20 mL of contrast material delivered at 2-3 mL/sec followed by 20 mL of saline solution delivered at the same rate. However, contrast material dosage and delivery rate should be adjusted with special attention to the acquisition time in individual patient. Several methods are used to determine the optimal delay between the start of intravenous contrast material injection and the start of image acquisition. Timing methods commonly used include a test bolus injection technique by using a small amount of contrast material, an automatic triggering technique (eg, Smart Prep; GE Medical Systems), and MR fluoroscopic technique [28-30].

Imaging interpretation is isually done with the aid of a computer workstation, on which individual source images were analyzed and postprocessing techniques were performed, such as multiplanar volume reformation, MIP reformation, and volume rendering of the images. Particularly, MIP images are quick to obtain, resemble catheter angiograms, and permit a 3D appreciation of anatomy (Fig. 3).

Aortic disease of the aorta

Aortic aneurysm

An aortic aneurysm is defined as a localized or diffuse dilatation involving all layers of the aortic wall and exceeding the expected aortic diameter by a factor of 1.5 or more [11]. Most thoracic and abdominal aneurysms are atherosclerotic in nature. Other causes of aortic

aneurysms include infection, inflammation, syphilis, and cystic medial necrosis. Atherosclerotic aneurysms are usually fusiform, although saccular aneurysms are occasionally encountered.

The major goal in imaging of an aortic aneurysm is the exact evaluation of the maximal diameter, the length, and involvement of major branch vessels [31]. All of these imaging features can be identified and characterized with MR imaging. Additionally, MR imaging can frequently be used as a follow-up tool for monitoring the progression of disease due to its high level of reproducibility of measurements. To obtain consistent results, vessel dimensions should be measured at the same anatomical locations between two subsequent examinations. Use of the sagittal or oblique sagittal plane allows the accurate assessment of location and extent of the aneurysm, and avoid partial volume effects. 3D contrast-enhanced MR angiography is most suitable for depicting location, extent, and exact diameter. This technique can provide precise topographic information concerning the extent of an aneurysm and its relationship to the aortic branches [24, 26, 32-33]. Although the resolution of contrast-enhanced MR angiography remains lower than that of multidetector CT, this technique is useful especially in patients with contraindications to iodinated contrast material. It is essential to recognize that measurement should be obtained from source images where the vessel wall is visible since MIP images represent a cast of the lumen alone (Fig. 4). Standard SE images are also helpful in evaluating changes in the aortic wall and periaortic structures. Area of high signal intensity on SE images within the thrombus and aortic wall may indicate instability of the aneurysm (Fig. 5, 6) [8]. Infected aneurysms result in fragility of the vessel wall by a bacterial infection, thus causing saccular outpouching, most commonly involving the suprarenal portion of the aorta. In this condition, MR imaging can demonstrate not only the aneurysm itself but also wall thickening and periaortic abscess (Fig. 7) [34, 35]. Inflammatory abdominal aortic aneurysm is a variant of atherosclerotic aneurysm, characterized by inflammatory and/or fibrotic changes in the periaortic lesions. In this condition, MR imaging shows homogenous periaortic tissue with sparing of the posterior aspect of the aorta. This periaortic tissue shows variable enhancement after injection of contrast material, based on the degree of inflammation and fibrosis (Fig. 8) [36,37]. Reduction in thickness of

periaortic tissue after surgical repair or endovascular stent-grafting is occasionally seen.

If an aneurysm involves the ascending aorta or sinuses of Valsalva, concomitant aortic valve disease can be evaluated using cine MR technique. As described in the literature, the capability of contrast MR angiography to visualize the Adamkiewicz artery provide an important information in planning the surgical repair of an aneurysm, thus avoiding postoperative neurological deficit secondary to spinal cord ischemia [38,39].

Aortic dissection

Aortic dissection is a life-threatening condition requiring prompt diagnosis and treatment. This condition occurs when blood dissects into the media of the aortic wall through an intimal tear. Classification of aortic dissections has been based traditionally on anatomical location (Stanford or DeBakey classification) and time from onset. The 14-day period after onset has been designated as the acute phase, because morbidity and mortality (15 – 25%) rates are highest and surviving patients typically stabilize during this period. The Stanford classification simply distinguishes aortic dissection irrespective of the site of the entry tear into type A if the ascending aorta is involved and type B if the ascending aorta is spared. This classification is fundamentally based on prognostic factors: type A dissection necessitates urgent surgical repair while most of type B dissection can be successfully managed conservatively. Hence, accurate recognition of anatomic details of the dissection with imaging is essential for successful management [40].

In dissection, the diagnostic goal is not only a clear anatomic delineation of the intimal flap and its extension, but also the detection of the entry and reentry sites and branch vessel involvement. MRI with current technology is the most accurate tool for detection of these imaging features of the dissection. High spatial and contrast resolution and multiplanar acquisition provide excellent sensitivity and specificity of the disease, and functional information with a totally non-invasive approach. In a patient with suspected aortic dissection, the MRI examination usually begins with spin echo “black blood” sequences, and the intimal flap is depicted as a linear structure in these sequences (Fig. 9). The true lumen can be differentiated from the false lumen by the following

findings: the true lumen shows a signal void, while the false lumen shows a higher signal intensity indicative of turbulent flow [41]. High signal intensity of pericardial effusion indicates a bloody component and is considered a sign of impending rupture of the ascending aorta into the pericardial space.

In stable patients, adjunctive gradient-echo sequences or phase contrast images can be performed in identifying aortic insufficiency and intimal tear sites as well as in differentiating slow flow from thrombus in the false lumen (Fig. 9). Further diagnostic refinement has been reported by gadolinium-enhanced 3D MR angiography in the diagnosis of aortic dissection and definition of its anatomic details [42]. Since 3D MR angiography is rapidly acquired without the need of ECG triggering, this technique may be performed even in severely ill patients. The lack of nephrotoxicity and other adverse effects enables the use of gadolinium in patients with renal failure or low cardiac output. The analysis of gadolinium-enhanced 3D MR angiography should not be restricted to viewing MIP images since MIP images occasionally fail to show the intimal flap (Fig. 10). It should also include a complete evaluation of reformatted images in all three planes in order to confirm or improve spin echo information and exclude artifacts. Combining the spin echo images with gadolinium-enhanced 3D MR angiography images completes the diagnosis and anatomical definition [43].

Intramural hematoma

Intramural hematoma is atypical form of dissection without flow in the false lumen or a discrete intraluminal flap [44, 45]. Intramural hematoma usually results from spontaneous rupture of the aortic wall vasa vasorum or from a penetrating atherosclerotic ulcer. Since clinical signs and symptoms and the prognosis of this condition do not differ to classic aortic dissection, its standard treatment is considered to be similar to that of classic aortic dissection [44]. Complete resolution of the aortic hematoma is occasionally seen. However, complications such as fluid extravasation with pericardial, pleural, and periaortic hematoma or aortic rupture may occur at the time of the onset or during the follow-up period.

Intramural hematoma can be identified as crescent thickening of the aortic wall with abnormal signal intensity. Because of the short T1-relaxation time of fresh blood, differentiation from the adjacent mediastinal fat may be difficult. In such circumstances, precontrast fat saturation images can be helpful in differentiating intramural hematoma from surrounding mediastinal fat. Moreover, MRI may allow the assessment of the age of hematoma on the basis of the different degradation products of hemoglobin. T1-weighted spin-echo MR image may show intermediate signal intensity due to presence of oxyhemoglobin in the acute stage, while it may show high signal intensity due to presence of methemoglobin in the subacute stage (Fig. 11) [8, 46]. The progression of intramural hematoma to overt dissection and rupture has been reported in 32% of the cases, particularly in cases with the involvement of ascending aorta.

Penetrating atherosclerotic ulcer

Penetrating atherosclerotic ulcer is characterized by ulceration of an atherosclerotic plaque that disrupting the intima [47,48]. The ulcerated atheroma may extend into the media, resulting in an intramural hematoma, or it may penetrate through the media and form a saccular pseudoaneurysm with the risk of transmural aortic rupture. Penetrating atherosclerotic ulcer usually affects elderly individuals with hypertension and extensive aortic atherosclerosis. It is typically located in the descending aorta, but locations in the aortic arch or in the abdominal aorta have been occasionally reported. Penetrating atherosclerotic ulcer should be considered a distinct entity with different management and prognosis although clinical features of this condition may be similar to those of aortic dissection. Persistent pain, hemodynamic instability, and signs of expansion are indications for surgical treatment, while asymptomatic patients can be managed medically and followed up with imaging. The diagnostic MR finding of penetrating atherosclerotic ulcer is the visualization of crater-like outpouching extending beyond the contour of the aortic lumen [48-50]. Mural thickening with high or intermediate signal intensity on spin echo sequences indicates the formation of intramural hematoma. On MR angiography, the penetrating atherosclerotic ulcer is readily recognized as a contrast-filled outpouching with jagged edge (Fig. 12). The disadvantage of MRI

compared with CT is inability to visualize dislodgment of intimal calcification, frequently seen in penetrating atherosclerotic ulcer.

Takayasu arteritis

Takayasu arteritis is an idiopathic large vessel vasculitis affecting the aorta and its major branches as well as pulmonary arteries. Etiology of Takayasu arteritis is still unknown although an autoimmune mechanism has been suspected. The arteritis is most common in Japan and other oriental countries, although now known worldwide. Women are affected about 10 times more often than men. Young women are particularly susceptible to the disease. Steno-occlusive lesions are characteristics of this disorder, but dilated forms are not also uncommon. Fever, malaise, easy fatigability, weakness of the upper extremity, dizziness, headache and syncope are the symptoms frequently complained. There are many synonyms including aortitis syndrome, aortic arch syndrome, pulseless disease, and young female arteritis.

Angiography used to be the gold standard to delineate the vascular abnormalities. However, CT and MRI are now considered to be the alternative noninvasive techniques [51-53]. In fact, they provide more information about vascular changes in Takayasu arteritis. Namely, the thickness of the vessel wall is better demonstrated by these new modalities. MR imaging provides the advantages of direct imaging in the axial, sagittal, and coronal planes, with good contrast resolution between the arterial lumen and its wall without use of contrast material.

The significant finding of acute-phase Takayasu arteritis is wall thickening of the aorta and its branches and the pulmonary arteries, which can be better visualized with multisectinal scanning by MR imaging. Wall thickening of the vertically positioned aorta can be seen best on axial images, while that of the horizontal portion of the right pulmonary artery can be evaluated best in the coronal and sagittal planes. Dramatic reduction of wall thickening in the aorta and pulmonary artery following steroid therapy may be documented by MR imaging (Fig. 13) [54].

In late occlusive phase, 3D contrast-enhanced MR angiography can reveal short or long-segment stenoses in the descending thoracic and abdominal aorta, and major branch vessels (Fig. 14). The

stenosing variety of late-phase Takayasu arteritis is known as atypical coarctation of the aorta (Fig. 15). The pulmonary arterial involvement with its incidence of approximately 70% can also be depicted by 3D contrast-enhanced MR angiography or contrast-enhanced MR perfusion imaging (2D fast spoiled gradient echo sequence with single-slice technique) (Fig. 16) [55].

References

[1] Flamm SD, VanDyke CW, White RD. MR imaging of the thoracic aorta. Magn Reson Imaging Clin N Am 1996;4:217-35.

[2] Leung DA, Debatin JF. Three-dimentional contrast-enhanced MRA of the thoracic vasculature. Eur Radiol 1997;7:981-9.

[3] Krinsky G, Reuss PM. MR angiography of the thoracic aorta. Magn Reson Imaging Clin N Am 1998;6:293-320

[4] Reddy GP, Higgins CB. MR imaging of the thoracic aorta. Magn Reson Imaging Clin N Am 2000;8:1-15.

[5] Ho VB, Corse WR, Hood MN, et al. MRA of the thoracic vessels. Semin Ultrasound CT MR 2003;24:192-216.

[6] Tatli S, Lipton MJ, Davison BD, et al. MR imaging of aortic and peripheral vascular disease. RadioGraphics 2003;23:S59-S78.

[7] Czum JM, Corse WR, Ho VB. MR angiography of the thoracic aorta. Magn Reson Imaging Clin N Am 2005;13:41-64.

[8] Russo V, Renzulli M, Buttazzi K, et al. Acquired diseases of the thoracic aorta: role of MRI and MRA. Eur Radiol 2006;16:852-865.

[9] Glazier HS, Gutierrez FR, Levitt G, et al. The thoracic aorta studied by MR imaging. Radiology 1985;157:149-55.

[10] Gomes AS. MR imaging of congenital anomalies of the thoracic aorta and pulmonary arteries. Radiol Clin North Am 1989;27:1171-81.

[11] Fattori R, Nienaber CA. MRI of acute and chronic aortic pathology: pre-operative and

postoperative evaluation. J Magn Reson Imaging 1999;10:741-750.

[12] Russo V, Renzulli M, Palombara CL, et al. Congenital diseases of the thoracic aorta: role of MRI and MRA. Eur Radiol 2006;16:676-684.

[13] Simonetti OP, Finn JP, White RD, et al. “Black blood” T2-weighted inversion recovery MR imaging of the heart. Radiology 1996;199:49-57.

[14] Pelc LR, Pelc NJ, Rayhill SC, et al. Arterial and venous blood flow: noninvasive quantification with MR imaging. Radiology 1992;185:809-12.

[15] Rebergen SA, van der Wall EE, Doornbos J, et al. Magnetic resonance measurement of velocity and flow: technique, validation, and cardiovascular application. Am Heart J 1993;126:1439-56.

[16] Earls JP, Ho VB, Foo TK, et al. Cardiac MRI: recent progress and continued challenges. J Magn Reson Imaging 2002; 16:111-27.

[17] Pereles FS, McCarthy RM, Baskaran V, et al. Thoracic aortic dissection and aneurysm: evaluation with nonenhanced true FISP MR angiography in less than 4 minutes. Radiology 2002;223:270-4.

[18] Prince MR, Yucel EK, Kaufman JA, et al. Dynamic gadolinium-enhanced three-dimensional abdominal MR arteriography. J Magn Reson Imaging 1993;3:877-881.

[19] McCauley TR, Monib A, Dickey KW, et al. Peripheral vascular occlusive disease: accuracy and reliability of time-of-flight MR angiography. Radiology 1994; 192:351-357.

[20] Didier D, Ratib O, Friedli B, et al. Cine gradient-echo MR imaging in the evaluation of cardiovascular disease. Radiographics 1993;13:561-73.

[21] Ho VB, Kinney JB, Sahn DJ. Contributions of newer MR imaging strategies for congenital heart disease. Radiographics 1996;16:43-60.

[22] Niezen RA, Doombos J, van der Wall EE, et al. Measurement of aortic and pulmonary flow with MRI at rest and during physical exercise. J Comput Assist Tomogr 1998;22:194-201.

[23] Powell AJ, Maier SE, Chung T, et al. Phase-velocity cine magnetic resonance imaging measurement of pulsatile blood flow in children and young adults: in vitro and in vivo validation.

Pediatr Cardiol 2000;21:104-110.

[24] Prince MR, Narasimham DL, Jacoby WT, et al. Three dimensional gadolinium-enhanced MR angiography of the thoracic aorta. Am J Roentgenol 1996;166:1387-1397.

[25] Krinsky G, Rofsky N, Flyer M, et al. Gadolinium-enhanced three dimensional MR angiography of acquired arch vessels disease. Am J Roentgenol 1996;167:981-987.

[26] Krinsky G, Rofsky N, De Corato DR, et al. Thoracic aorta: comparison of gadolinium-enhanced three dimensional MR angiography with conventional MR imaging. Radiology 1997;202:183-193.

[27] Svensson J, Petersson JS, Stahlberg F, et al. Image artifacts due to a time-varying contrast medium concentration in 3D contrast-enhanced MRA. J Magn Reson Imaging 1999;10:919-928.

[28] Hany TF, Mckinnon GC, Leung DA, et al. Optimization of contrast timing for breath-holding three-dimensional MR angiography. J Magn Reson Imaging 1997;7:551-556.

[29] Foo TK, Saranathan M, Prince MR, et al. Automated detection of bolus arrival and initiation of data acquisition in fast, three-dimensional, gadolinium-enhanced MR angiography. Radiology 1997;203:275-280.

[30] Riederer SJ, Bernstein MA, Breen JF, et al. Three-dimensional contrast-enhanced MR angiography with real-time fluoroscopic triggering: design specifications and technical reliability in 330 patient studies. Radiology 2000;215:584-593.

[31] Bonser RS, Pagano D, Lewis ME, et al. Clinical and patho-anatomical factors affecting expansion of thoracic aortic aneurysms. Heart 2000;84:277-283.

[32] Debatin JF, Hany TF. MR-based assessment of vascular morphology and function. Eur Radiol 1998;8:528-539.

[33] Neimatallah MA, Ho VB, Dong Q, et al. Gadolinium-based 3D magnetic resonance angiography of the thoracic vessels. J Magn Reson Imaging 1999;10:758-770.

[34] Sueyoshi E, Sakamoto I, Kawahara Y, et al. Infected abdominal aortic aneurysm: early CT findings. Abdom Imaging. 1998;23:645-8.

[35] Macedo TA, Stanson AW, Oderich GS, et al. Infected aortic aneurysms: imaging findings.

Radiology 2004;231:250-7.

[36] Berletti R, D'Andrea P, Cavagna E, et al. Inflammatory and fibrotic changes in the periaortic regions: integrated US, CT and MR imaging in three cases. Radiol Med 2002;103:427-32.

[37] Anbarasu A, Harris PL, McWilliams RG. The role of gadolinium-enhanced MR imaging in the preoperative evaluation of inflammatory abdominal aortic aneurysm. Eur Radiol 2002;12:S192-5.

[38] Nijenhuis RJ, Jacobs MJ, van Engelshoven JM, et al. MR angiography of the Adamkiewicz artery and anterior radiculomedullary vein: postmortem validation. AJNR Am J Neuroradiol 2006;27:1573-5.

[39] Yoshioka K, Niinuma H, Ehara S, et al. MR Angiography and CT Angiography of the Artery of Adamkiewicz: State of the Art. Radiographics 2006;26:S63-73.

[40] Cigarroa JE, Isselbacher EM, DeSanctis RW, et al. Diagnostic standard and new direction. N Engl J Med 1993;328:35-43.

[41] Chang JM, Friese K, Caputo GR, et al. MR measurement of blood flow in the true and false channel in chronic aortic dissection. J Comput Assist Tomogr 1991;15:418-423.

[42] Fisher U, Vossherich R, Kopka L, et al. Dissection of the thoracic aorta: pre- and postoperative findings of turbo-FLASH MR images in the plane of the aortic arch. Am J Roentgenol 1994;163:1069-1072.

[43] Bogaert J, Meyns B, Rademakers FE, et al. Follow-up of aortic dissection: contribution of MR angiography for evaluation of the abdominal aorta and its branches. Eur Radiol 1997;7:695-702.

[44] Nienaber CA, von Kodolitsch Y, Petersen B, et al. Intramural hemorrhage of the thoracic aorta: diagnosis and therapeutic implications. Circulation 1995;92:1465-1472.

[45] Ganaha F, Miller DC, Sugimoto K, et al. Prognosis of aortic intramural hematoma with and without penetrating atherosclerotic ulcer: a clinical and radiological analysis. Circulation 2002;106:342-348.

[46] Murray JG, Manisali M, Flamm SD, et al. Intramural hematoma of the thoracic aorta: MR imaging findings and their prognostic implications. Radiology 1997;204:349-355.

[47] Stanson AW, Kazmier FJ, Hollier LH, et al. Penetrating atherosclerotic ulcers of the thoracic

aorta: natural history and clinicopathologic correlations. Ann Vasc Surg 1986;1:15-23.

[48] Hayashi H, Matsuoka Y, Sakamoto I, et al. Penetrating atherosclerotic ulcer of the aorta: imaging features and disease concept. Radiographics. 2000;20:995-1005.

[49] Macura KJ, Szarf G, Fishman EK, et al. Role of computed tomography and magnetic resonance imaging in assessment of acute aortic syndromes. Semin Ultrasound CT MR. 2003;24:232-54.

[50] Yucel EK, Steinberg FL, Egglin TK, et al. Penetrating aortic ulcers: diagnosis with MR imaging. Radiology. 1990;177:779-81.

[51] Matsunaga N, Hayashi K, Sakamoto I, et al. Takayasu arteritis: Protean radiologic manifestations and diagnosis. Radiographics 1997;17:579-594.

[52] Matsunaga N, Hayashi K, Okada M, et al. Magnetic resonance imaging features of aortic diseases. Top Magn Reson Imaging 2003;14:253-66.

[53] Nastri MV, Baptista LP, Baroni RH, et al. Gadolinium-enhanced three-dimensional MR angiography of Takayasu arteritis. Radiographics. 2004;24:773-86

[54] Tanigawa K, Eguchi K, Kitamura Y, et al. Magnetic resonance imaging detection of aortic and pulmonary artery wall thickening in acute stage of Takayasu arteritis: Improvement of clinical and radiologic findings after steroid therapy. Arthritis Rheum 1992;35:476-480.

[55] Sueyoshi E, Sakamoto I, Ogawa Y, et al. Diagnosis of perfusion abnormality of the pulmonary artery in Takayasu's arteritis using contrast-enhanced MR perfusion imaging. Eur Radiol. 2006;16:1551-6.

Figure legends

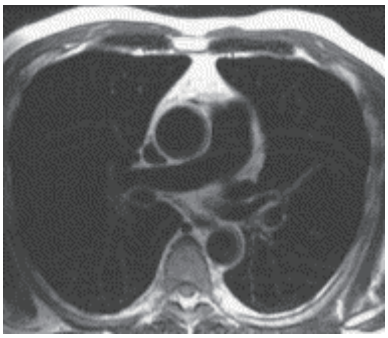

Figure 1. Black-blood imaging of the aorta obtained at the level of the right pulmonary artery. Note the excellent suppression of the luminal blood signal and demonstration of the vessel wall. The image was obtained in 12 seconds with cardiac gating and breath holding.

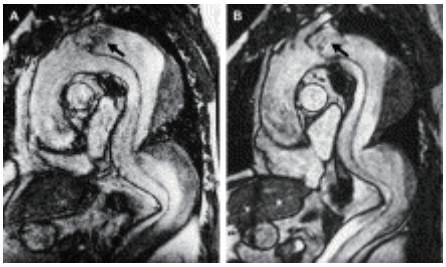

Figure 2. Cine MR imaging in a patient with aortic dissection. Sagittal cine MR imaging obtained with standard gradient echo pulse sequence and during free breathing (A) more clearly reveals a flow jet (arrows) through the entry than that obtained with SSFP sequence and during breath holding (B).

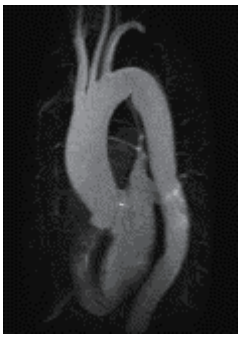

Figure 3. 3D contrast-enhanced MR angiography of the thoracic aorta. Oblique sagittal MIP image clearly depicts the entire thoracic aorta and branch vessels from the aortic arch.

Fig 4. 3D contrast-enhanced MR angiography in a patient with aortic arch aneurysm. Source image of 3D contrast-enhanced MR angiography (A) more clearly depicts involvement of the left subclavian artery by an aortic arch aneurysm than MIP image (B). Arrows in A indicates the aortic arch aneurysm with mural thrombus. As described here, in aneurysms with a large volume of mural thrombus, accurate evaluation of the branch vessel involvement by the aneurysm is difficult or impossible by MIP images alone.

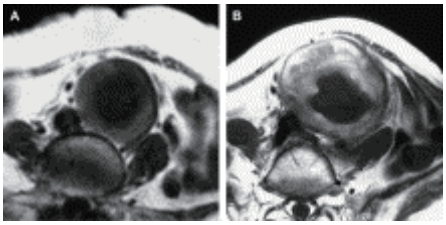

Fig. 5　Spin echo MR imaging of mural thrombus in impending rupture of an abdominal aortic aneurysm (AAA). T1-weighted spin echo MR image obtained 24 months before impending rupture (A) shows infrarenal AAA with mural thrombus of homogenous low intensity.　T1-weighted spin echo MR image obtained at the time of impending rupture (B) reveals an interval enlargement of the AAA. Partial area of high signal intensity is also noted within the mural thrombus. In this case, small amount of periaortic hemorrhage and hemorrhage into the mural thrombus were found at surgery.

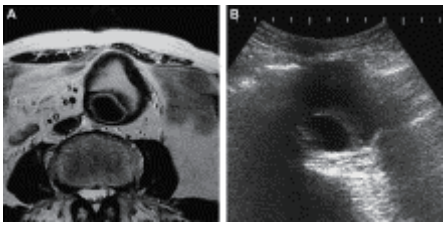

Fig. 6　Spin echo MR imaging of liquefactive thrombus in abdominal aortic aneurysm (AAA). Most of mural thrombus is markedly high in signal intensity on T2- weighted spin echo images (A). The high signal intense area in the mural thrombus is anechoic on US (B), indicating liquefaction of the thrombus.

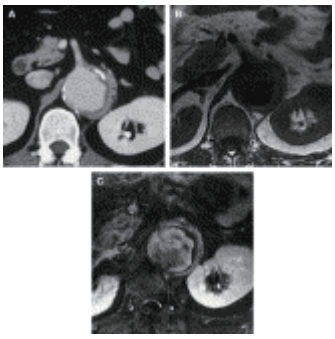

Fig. 7　MR imaging of infected aortic aneurysm. Contrast-enhanced CT (A) demonstrates an enlargement of the suprarenal abdominal aorta with a small amount of periaortic tissue adjacent to anterior to left lateral aspect of the aorta. Hyperenhancement of the periaortic tissue is also noted. T1-weighted spin echo MR images before (B) and after (C) injection of contrast material show the suprarenal abdominal aortic aneurysm with inhomogenous hyperenhancement of the periaortic tissue.

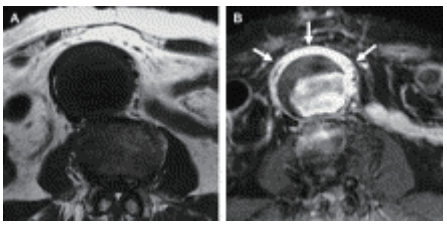

Fig. 8　MR imaging of inflammatory abdominal aortic aneurysm.　T1-weighted spin echo MR image (A) shows infrarenal abdominal aortic aneurysm and periaortic tissue with sparing of posterolateral aspect of the aorta. T1-weighted spin echo MR image after contrast material injection (B) shows homogenous hyperenhancement of the periaortic tissue (arrows), indicating periaortic fibrosis and inflammation.

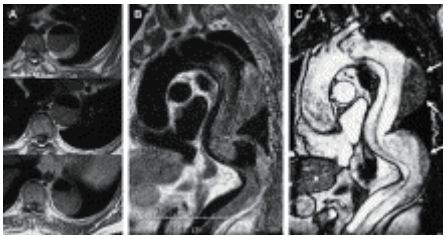

Fig. 9　MR imaging of aortic dissection.　Axial (A) and oblique sagittal (B) spin echo images of type B dissection shows a linear structure in the descending thoracic aorta, indicating the dissection flap. The true lumen is narrowed by compression of a dilated false lumen.　Note a higher signal intensity in the false lumen, indicating turbulent flow and/or thrombus in the false lumen. Turbulent flow in the false lumen cannot be differentiated from thrombus using spin echo techniques alone.　On oblique sagittal cine MR imaging with SSFP technique (C), flowing blood in the false and true lumens is visualized as high intensity, and partial thrombus in the false lumen as low intensity (arrows).

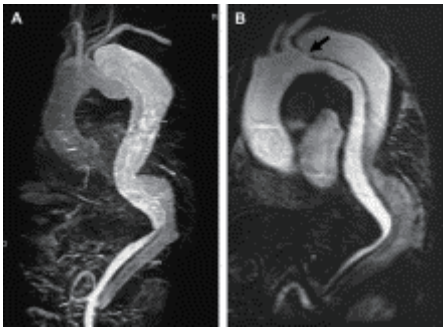

Fig. 10　3D contrast-enhanced MR angiography of aortic dissection.　The anatomical details of the dissected aorta are difficult to recognize on MIP image of 3D contrast-enhanced MR angiography (A) alone.　Oblique sagittal reformatted image clearly depicts not only the intimal flap but also the entry site (arrow).

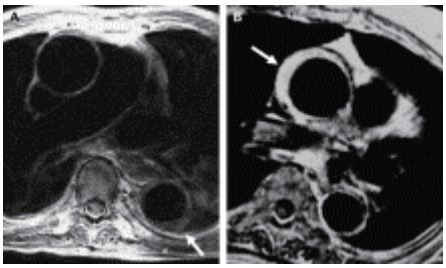

Fig. 11　Spin echo MR imaging of intramural hematoma.　On T1-weighted spin-echo MR image obtained 2 days after the onset (A), intramural hematoma of the descending thoracic aorta shows intermediate signal intensity (arrow) due to presence of oxyhemoglobin (acute stage).　On T1-weighted spin-echo MR image obtained 40 days after the onset (B, a different patient from A), intramural hematoma of the ascending thoracic aorta shows high signal intensity (arrow) due to presence of methemoglobin (subacute stage).

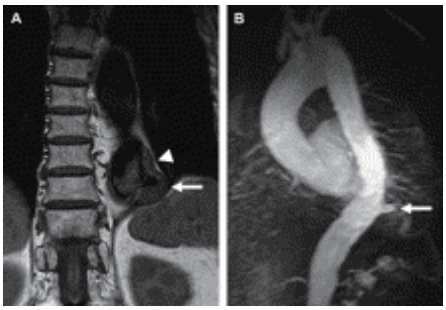

Fig. 12 MR imaging of penetrating atherosclerotic ulcer.　Sagittal T1-weighted spin-echo MR image (A) and MIP image of 3D contrast-enhanced MR angiography (B) clearly depict penetrating atherosclerotic ulcer in mid-portion of the descending thoracic aorta (arrow).　Note mural thickening with intermediate signal intensity (arrowhead in A) indicating the formation of intramural hematoma (A).

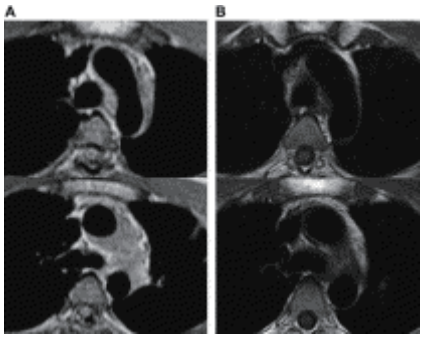

Fig. 13　Improvement of aortic wall thickening in early-phase Takayasu arteritis.　T1-weighted spin-echo MR images obtained before (A) and after (B) steroid therapy demonstrates marked reduction of the aortic wall thickening after steroid therapy.

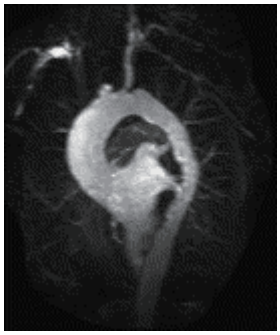

Fig. 14　3D contrast-enhanced MR angiography of late-phase Takayasu artreitis. MIP image of 3D contrast-enhanced MR angiography shows occlusion of the right brachiocephalic and right common carotid arteries, and mild stenosis of the orifice of the left subclavian artery. Note irregular and diffuse narrowing of proximal segment of the thoracic descending aorta.

Fig. 15　3D contrast-enhanced MR angiography of late-phase Takayasu artreitis.　MIP image of 3D contrast-enhanced MR angiography shows marked and irregular narrowing of the abdominal aorta.　This stenosing type of late-phase Takayasu artreitis is known as atypical coarctation of the aorta.

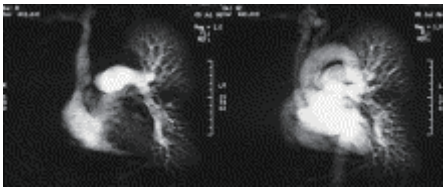

Fig. 16　Contrast-enhanced MR perfusion imaging of the lung in a patient with late-phase Takayasu artreitis.　Serial subtracted MR images of contrast-enhanced MR perfusion imaging of the lung show occlusion of the right main trunk of the pulmonary artery and a perfusion defect in the middle lung field of the left lung.